U-Mamba: Enhancing Long-range Dependency for Biomedical Image Segmentation

Jun Ma[1,2,3], Feifei Li[1], and Bo Wang[1,2,3,4,5]

[1] Peter Munk Cardiac Centre, University Health Network, Toronto, Canada
[2] Department of Laboratory Medicine and Pathobiology, University of Toronto, Toronto, Canada
[3] Vector Institute for Artificial Intelligence, Toronto, Canada
[4] Department of Computer Science, University of Toronto, Toronto, Canada
[5] AI Hub, University Health Network, Toronto, Canada
`bowang@vectorinstitute.ai`

Abstract. Convolutional Neural Networks (CNNs) and Transformers have been the most popular architectures for biomedical image segmentation, but both of them have limited ability to handle long-range dependencies because of inherent locality or computational complexity. To address this challenge, we introduce U-Mamba, a general-purpose network for biomedical image segmentation. Inspired by the State Space Sequence Models (SSMs), a new family of deep sequence models known for their strong capability in handling long sequences, we design a hybrid CNN-SSM block that integrates the local feature extraction power of convolutional layers with the abilities of SSMs for capturing the long-range dependency. Moreover, U-Mamba enjoys a self-configuring mechanism, allowing it to automatically adapt to various datasets without manual intervention. We conduct extensive experiments on four diverse tasks, including the 3D abdominal organ segmentation in CT and MR images, instrument segmentation in endoscopy images, and cell segmentation in microscopy images. The results reveal that U-Mamba outperforms state-of-the-art CNN-based and Transformer-based segmentation networks across all tasks. This opens new avenues for efficient long-range dependency modeling in biomedical image analysis. The code, models, and data are publicly available at `https://wanglab.ai/u-mamba.html`.

Keywords: Image Segmentation · Backbone Network · State Space Models · Transformer.

1 Introduction

Segmentation serves as a foundational process in biomedical image analysis that divides images into meaningful anatomical structures or areas of interest for doctors and biologists. This task is crucial in various biomedical applications [38,33], such as diagnosing diseases, quantifying cancer microenvironments, planning

treatment strategies, and tracking disease progression. Manual segmentation is a straightforward way for this task but it is extremely time-consuming and requires extensive domain knowledge, which is impractical in practice. Thus, there is a great demand for automatic segmentation methods. During the past ten years, segmentation methodology has undergone a paradigm shift from Mathematical model- or hand-crafted feature-based approaches to deep learning-based paradigm, which significantly improved the segmentation accuracy and efficiency for a broad range of biomedical tasks, such as tumor segmentation [3,19] and organ segmentation [35] in 3D Computed Tomograph (CT) scans, as well as cell segmentation in microscopy images [43,34].

Two popular network architectures, CNNs [27] and Transformers [46], have gained prominence in medical image segmentation. CNNs, such as U-Net [41,22] and DeepLab [7], are efficient in extracting hierarchical image features and more parameter-efficient than naïve fully connected networks. Their shared weights architecture makes them excel at capturing translational invariances and recognizing local features. Transformers were originally designed for natural language processing, but have been successfully adapted for image processing, such as Vision Transformer (ViT) [9] for image recognition and SwinTransformer [28] for a general backbone in various vision tasks. In contrast to CNNs, Transformers do not inherently process spatial image hierarchies but treat the image as a sequence of patches. which has better capabilities to capture global information. Due to this complementary feature, many studies have explored incorporating Transformers into CNNs via hybrid network architectures, such as TransUNet [5,6], UNETR [17], nnFormer [49], and SwinUNETR [16].

While Transformers have improved the ability of long-range dependencies, they are generally very computationally expensive. This is because the self-attention mechanism scales quadratically with the input size, making them resource-intensive, especially for biomedical images that usually have high resolutions. Thus, how to efficiently enhance the long-range dependency in CNNs remains an open question. Recently, state space sequence models (SSMs) [11,15], in particular structured state space sequence models (S4) [14], have emerged as an efficient and effective building block (or layer) for constructing deep networks, which obtained cutting-edge performance in continuous long-sequence data analysis [10,14]. Mamba [12] further improved S4 with a selective mechanism, allowing the model to select relevant information in an input-dependent manner. By combining with hardware-aware implementation, Mamba surpassed Transformers on dense modalities such as language and genomics. On the other hand, state space models also have shown promising results on vision tasks, such as images [40] and videos [24] classification. Since image patches and image features can be cast as sequences [9,28], these appealing features of SSMs motivated us to explore the potential of using Mamba blocks to enhance the long-range modeling ability in CNNs.

In this paper, we propose U-Mamba, a general-purpose network, for both 3D and 2D biomedical image segmentation. Based on the innovative hybrid CNN-SSM architecture, U-Mamba can capture both localized fine-grained features

and long-range dependencies in images. This network stands out from prevalent Transformer-based architectures by offering linear scaling in feature size, as opposed to the quadratic complexity often associated with Transformers. Additionally, U-Mamba's self-configuring capability enables seamless adaptation to various datasets, enhancing its scalability and flexibility across a spectrum of biomedical segmentation tasks. Quantitative and qualitative results on four distinct datasets demonstrate that U-Mamba achieves superior performance, surpassing Transformer-based networks by a large margin. This paves the way for future advancements in network designs that efficiently and effectively model long-range dependencies in biomedical imaging.

2   Method

U-Mamba follows the encoder-decoder network structure that captures both local features and long-range contexts in an efficient way. Fig. 1 shows an overview of the U-Mamba block and the complete network structure. Next, we first introduce the Mamba block followed by illustrating the details of U-Mamba.
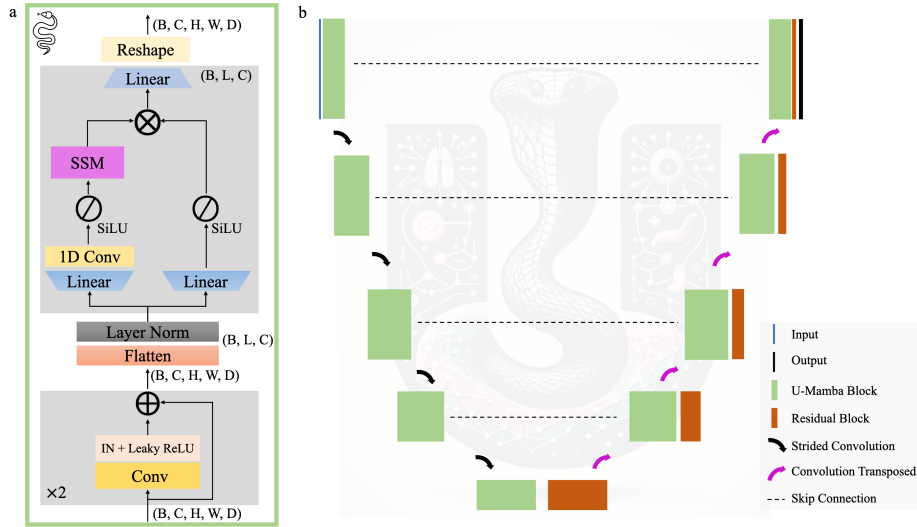

Fig. 1. Overview of the U-Mamba (Enc) architecture. **a,** U-Mamba building block contains two successive Residual blocks followed by the SSM-based Mamba block for enhanced long-range dependency modeling. **b,** U-Mamba employs the encoder-decoder framework with U-Mamba blocks in the endocer, Residual blocks in the decoder, together with skip connections. Note: This illustration serves as a conceptual representation. U-Mamba inherits the self-configuring feature from nnU-Net and the number of network blocks is automatically determined across datasets. The detailed network configurations are presented in Table 2.

2.1   Mamba: Selective Structured State Space Sequence Models with a Scan (S6)

State Space Sequence Models (SSMs) [11] are a type of systems that map a 1-dimensional function or sequence $u(t) \mapsto y(t) \in \mathrm{R}$ and can be represented as the following linear Ordinary Differential Equation (ODE):

$$\begin{aligned} x'(t) &= \mathbf{A}x(t) + \mathbf{B}u(t), \\ y(t) &= \mathbf{C}x(t), \end{aligned} \tag{1}$$

where state matrix $A \in \mathrm{R}^{N \times N}$ and $B, C \in \mathrm{R}^N$ are its parameters and $x(t) \in \mathrm{R}^N$ denotes the implicit latent state. SSMs offer several desired properties, such as linear computational complexity per time step and parallelized computation for efficient training. However, naïve SSMs typically demand more memory than equivalent CNNs and often encounter vanishing gradients during training, hindering their broader application in general sequence modeling.

Structured State Space Sequence Models (S4) [14] significantly improve the naïve SSMs by imposing structured forms on the state matrix $\mathbf{A}$ and introducing an effective algorithm. Specifically, the state matrix is crafted and initialized with High-Order Polynomial Projection Operator (HIPPO) [13], allowing to building deep sequence models with rich capability and efficient long-range reasoning ability. S4, as a new type of network architecture, has surpassed Transformers [46] on the challenging Long Range Arena Benchmark [44] by a significant margin.

Recently, Mamba [12] further advances SSMs in discrete data modeling (e.g., text and genome) through two key improvements. First, Mamba employs an input-dependent selection mechanism, distinct from the traditional time- and input-invariant SSMs, which allows for efficient information filtering from inputs. This is implemented by parameterizing the SSM parameters based on the input data. Second, a hardware-aware algorithm, scaling linearly in sequence length, is developed to compute the model recurrently with a scan, making Mamba faster than previous methods on modern hardware. In addition, The Mamba architecture, merging SSM blocks with linear layers, is notably simpler and has demonstrated state-of-the-art performance in various long-sequence domains including language and genomics, showcasing significant computational efficiency during both training and inference.

2.2   U-Mamba: Marry Mamba with U-Net

Mamba has demonstrated impressive results on various discrete data, yet its potential for modeling image data, particularly in biomedical imaging, remains underexplored. Given that images are essentially discrete data sampled from continuous signals and can be treated as long sequences when flattened, we propose leveraging Mamba's linear scaling advantage to enhance CNNs' long-range dependency modeling. Transformers have been successfully applied to handle images, such as ViT [9] and SwinTransformer [28], but they often suffer from high computational burden for large images because self-attention [46] has quadratic

complexity. These factors motivate us to leverage the linear scaling property in Mamba to enhance the long-range dependency of CNNs.

U-Net [41] and its variants [22] have been the widely used network architecture in medical image segmentation. They usually have symmetric encoder-decoder architecture to extract multi-scale image features with convolutional operations. However, this architectural design has limited ability to model long-range dependencies in images because convolutional kernels are inherently local. Each convolutional layer captures features from a limited receptive field. While skip connections in U-Net help in combining low-level details with high-level features, they primarily reinforce local feature integration rather than expanding the network's ability to model long-range dependencies.

U-Mamba is designed to acquire the best of U-Net and Mamba for global context understanding in medical image segmentation. As shown in Fig. 1a, each building block contains two successive Residual blocks [18] followed by a Mamba block [12]. The Residual block contains the plain convolutional layer followed by Instance Normalization (IN) [45] and Leaky ReLU [36]. Image features with a shape of (B, C, H, W, D) are then flattened and transposed to (B, L, C) where $L = H \times W \times D$. After passing the Layer Normalization [2], the features enter the Mamba block that contains two parallel branches. In the first branch, the features are expanded to $(B, 2L, C)$ by a linear layer followed by a 1D convolutional layer, SiLU activation function [20], and together with the SSM layer. In the second branch, the features are also expanded to $(B, 2L, C)$ with a linear layer followed by the SiLU activation function. After that, the features from the two branches are merged with the Hadamard product. Finally, the features are projected back to the original shape (B, L, C) and then reshaped and transposed to (B, C, H, W, D).

Fig. 1b shows the complete U-Mamba network architecture where the encoder is built with the above blocks to capture both local features and long-range dependencies. The decoder, composed of Residual blocks and transposed convolutions, focuses on detailed local information and resolution recovery. Moreover, we inherit the skip connection in U-Net to connect the hierarchical features from the encoder to the decoder. The final decoder feature is passed to a $1 \times 1 \times 1$ convolutional layer together with a Softmax layer to produce the final segmentation probability map. In addition, we also implement a U-Mamba variant where only the bottleneck uses the U-Mamba block and the others are plain Residual blocks. We use "U-Mamba_Bot" and "U-Mamba_Enc" to differentiate the two network variants, which employ the U-Mamba block in the bottleneck and all encoder blocks, respectively.

3   Experiments and results

3.1   Datasets

We used four medical image datasets to evaluate the performance and scalability of U-Mamba across different image sizes, segmentation targets, and modalities.

Table 1 presents an overview of the datasets. All the datasets are publicly available and allowed for research purposes.

Table 1. Dataset information.

Dataset	Dimension	#Training Image	#Testing Image	#Targets
Abdomen CT	3D	50 (4794 slices)	50 (10894 slices)	13
Abdomen MRI	3D	60 (5615 slices)	50 (3357 slices)	13
Endoscopy Images	2D	1800	1200	7
Microscopy Images	2D	1000	101	2

Abdomen CT: This dataset was from the MICCAI 2022 FLARE Challenge [35] that focused on the segmentation of 13 abdominal organs, including the liver, spleen, pancreas, right kidney, left kidney, stomach, gallbladder, esophagus, aorta, inferior vena cava, right adrenal gland, left adrenal gland, and duodenum. The training set contained 50 CT scans that were from the MSD Pancreas dataset [42] and the annotations were from AbdomenCT-1K. Another 50 cases from different medical centers [8] were used for evaluation and the annotations were provided by the challenge organizers.

Abdomen MRI: This dataset was from the MICCAI 2022 AMOS Challenge [25] that also focused on abdominal organ segmentation. The original dataset contains 40 and 20 MRI scans for training and validation, respectively. Since 20 cases are not enough to draw statistically meaningful results, in our experiments, we used the original 60 labeled MRI scans for model training and annotated another 50 MRI scans as the testing set. In order to enable modality-wise comparison of abdominal organs, we also focused on the same 13 organs as the Abdomen CT dataset. The annotations were generated by radiologists with the assistance of MedSAM [32] and ITK-SNAP [48]. We have released this new annotated dataset to the community to promote the development of abdominal organ segmentation in MRI.

Endoscopy images: This dataset was from the MICCAI 2017 EndoVis Challenge [1] that focused on segmenting seven instruments from endoscopy images, including the large needle driver, prograsp forceps, monopolar curved scissors, cadiere forceps, bipolar forceps, vessel sealer, and additionally a drop-in ultrasound probe. We followed the official dataset splitting where the training set contained 1800 and 1200 image frames, respectively. The training images were from eight videos while the testing set had unseen images from another two new videos.

Microscopy images: This dataset was from the NeurIPS 2022 Cell Segmentation Challenge [34] that focused on cell segmentation in various microscopy images. We used 1000 and 101 images for training and evaluation, respectively. Different from the above three tasks, this is an instance segmentation task where algorithms are expected to assign a unique label for each cell instance. In our experiments, we converted the instance segmentation into a semantic segmentation task by predicting the cell boundaries and interior regions because they can

be easily transformed to instance masks via the "skimage.measure.label" function. It should be noted that our purpose was to benchmark the performance of network architectures, rather than pursue state-of-the-art performance on this task. U-Mamba can also serve as a backbone network in state-of-the-art instance segmentation framework [34]. We leave this extension as future work.

3.2   Implementation and training protocols

We implemented U-Mamba within the popular nnU-Net [22] framework driven by two desired features. First, the modular design of nnU-Net aligns perfectly with our focus on introducing a new network architecture. This design allows us to concentrate on the network's implementation while controlling other variables, such as image preprocessing and data augmentation. Such a setup enables a fair comparison of U-Mamba against various methods under uniform conditions, with the network architecture being the only differing factor. Second, nnU-Net's notable self-configuring framework, capable of automatically configuring hyper-parameters for diverse segmentation datasets, is another compelling reason for our choice. We also preserve this feature, allowing U-Mamba to be easily adapted to a broad range of segmentation tasks. During training, the patch size, batch size, and network configurations (e.g., the number of resolution states and the number of downsampling operations along different axes) remained consistent with nnU-Net (Table 2). U-Mamba was also optimized with stochastic gradient descent and the loss function was the unweighted sum of Dice loss and cross-entropy because the compound loss has proven to be robust across different tasks [31]. During inference, the testing time augmentation (TTA) was disabled in all the experiments for a more streamlined and efficient evaluation process because TTA would increase the computational burden by $4\times$ and $8\times$ times for 2D and 3D datasets, respectively.

Table 2. U-Mamba configurations for each dataset.

Configurations	Patch size	Batch size	# Stages	# Pooling per axis
Abdomen CT	(40, 224, 192)	2	6	(3, 3, 5)
3D Abdomen MR	(48, 160, 224)	2	6	(3, 5, 5)
2D Abdomen MR	(320, 320)	30	7	(6, 6)
Endoscopy	(384, 640)	13	7	(6, 6)
Microscopy	(512, 512)	12	8	(7, 7)

3.3   Benchmarking

We compared U-Mamba with two CNN-based segmentation networks (nnU-Net [22] and SegResNet [39]) and two Transformer-based networks (UNETR [17] and SwinUNETR [16]), which are widely used in medical image segmentation competitions. For a fair comparison, we also implemented SegResNet, UNETR,

and SwinUNETR into the nnU-Net framework and used their suggested optimizers (e.g., Adam [26] and AdamW [29]) for model training. We used the default image preprocessing in nnU-Net [22]. All the networks were trained from scratch for 1000 epochs on one NVIDIA A100 GPU in the same batch size (Table 2).

Following the recommendations in Metrics Reloaded [37], we used Dice Similarity Coefficient (DSC) and Normalized Surface Distance (NSD) for three semantic segmentation tasks, including organ segmentation in CT and MRI scans, and instrument segmentation in Endoscopy images. F1 score was used to evaluate the cell segmentation quality because it is an instance segmentation task.

Table 3. Results summary of 3D organ segmentation on abdomen CT and MRI datasets. U-Mamba_Bot: only use the U-Mmaba block in the bottleneck. U-Mamba_Enc: all encoder blocks are U-Mmaba blocks.

Methods	Organs in Abdomen CT		Organs in Abdomen MRI	
	DSC	NSD	DSC	NSD
nnU-Net	0.8615±0.0790	0.8972±0.0824	0.8309±0.0769	0.8996±0.0729
SegResNet	0.7927±0.1162	0.8257±0.1194	0.8146±0.0959	0.8841±0.0917
UNETR	0.6824±0.1506	0.7004±0.1577	0.6867±0.1488	0.7440±0.1627
SwinUNETR	0.7594±0.1095	0.7663±0.1190	0.7565±0.1394	0.8218±0.1409
U-Mamba_Bot	**0.8683±0.0808**	**0.9049±0.0821**	**0.8453±0.0673**	**0.9121±0.0634**
U-Mamba_Enc	**0.8638±0.0908**	**0.8980±0.0921**	**0.8501±0.0732**	**0.9171±0.0689**

Ground Truth   nnU-Net   SegResNet   UNETR   SwinUNETR   U-Mamba_Bot   U-Mamba_Enc
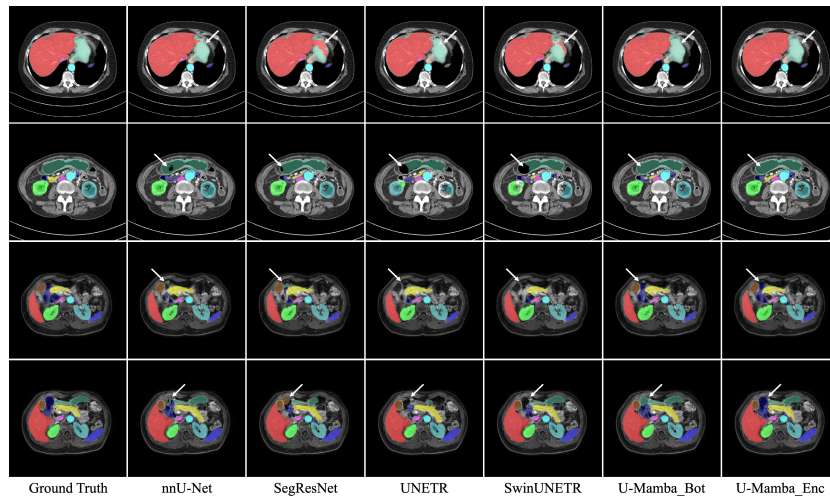
Fig. 2. Visualized segmentation examples of abdominal organ segmentation in CT (1st and 2nd rows) and MRI scans (3rd and 4th rows). U-Mamba has better capabilities to distinguish complex soft tissues in the abdomen.

3.4   Quantitative and qualitative segmentation results

Table 3 shows quantitative 3D segmentation results of abdominal organs in CT and MRI scans. U-Mamba surpasses both CNN and Transformer-based segmentation networks, achieving average DSC scores of 0.8683 (U-Mamba_Bot) and 0.8501 (U-Mamba_Enc) on the abdomen CT and MR datasets, respectively. nnU-Net performs competitively, which is much better than SegResNet, UNETR, and SwinUNETR, but U-Mamba still shows advantages as shown in Fig. 2. Based on the visualized segmentation results of the six networks, U-Mamba has fewer outliers in the segmentation results. For instance, U-Mama can generate more accurate liver and stomach segmentation masks while the others have over-segmentation errors for liver masks and missing regions for stomach masks in abdomen CT scans. Similarly, for gallbladder segmentation in MRI scans, U-Mamba successfully delineates its boundary while other methods generate various segmentation errors. These observations are also reflected in the organ-wise DSC and NSD scores (Appendix Table 5 and Table 6).

Table 4. Results summary of 2D segmentation tasks: organ segmentation in abdomen MRI scans, instruments segmentation in endoscopy images, and cell segmentation in microscopy images.

Methods	Organs in Abdomem MRI		Instruments in Endoscopy		Cells in Microscopy
	DSC	NSD	DSC	NSD	F1
nnU-Net	0.7450±0.1117	0.8153±0.1145	0.6264±0.3024	0.6412±0.3074	0.5383±0.2657
SegResNet	0.7317±0.1379	0.8034±0.1386	0.5820±0.3268	0.5968±0.3303	0.5411±0.2633
UNETR	0.5747±0.1672	0.6309±0.1858	0.5017±0.3201	0.5168±0.3235	0.4357±0.2572
SwinUNETR	0.7028±0.1348	0.7669±0.1442	0.5528±0.3089	0.5683±0.3123	0.3967±0.2621
U-Mamba_Bot	**0.7588±0.1051**	**0.8285±0.1074**	**0.6540±0.3008**	**0.6692±0.3050**	**0.5389±0.2817**
U-Mamba_Enc	**0.7625±0.1082**	**0.8327±0.1087**	**0.6303±0.3067**	**0.6451±0.3104**	**0.5607±0.2784**

   Table 4 presents quantitative 2D segmentation results. MRI scans usually have more heterogeneous spacing than CT scans and 2D segmentation networks are also a common choice in practice [4]. Thus, we also compared all the networks under the 2D setting for abdominal organ segmentation where each 3D MRI scan was converted into multiple 2D slices. U-Mamba again demonstrates its advantages over existing methods on the three 2D segmentation tasks, achieving the best average DSC of 0.7625, 0.6504, and F1 score of 0.5607 for organs, instruments, and cell segmentation, respectively. Qualitative results in Fig. 2 show that nnU-Net, UNETR, and SwinUNETR confuse the spleen because of heterogeneous appearances. UNETR and SwinUNETR also generate many cell outliers in the microscopy image and nnU-Net failed to successfully recognize the large needle driver in the endoscopy image. In contrast, U-Mamba shows clear advantages across these scenarios, indicating better abilities to capture global context.
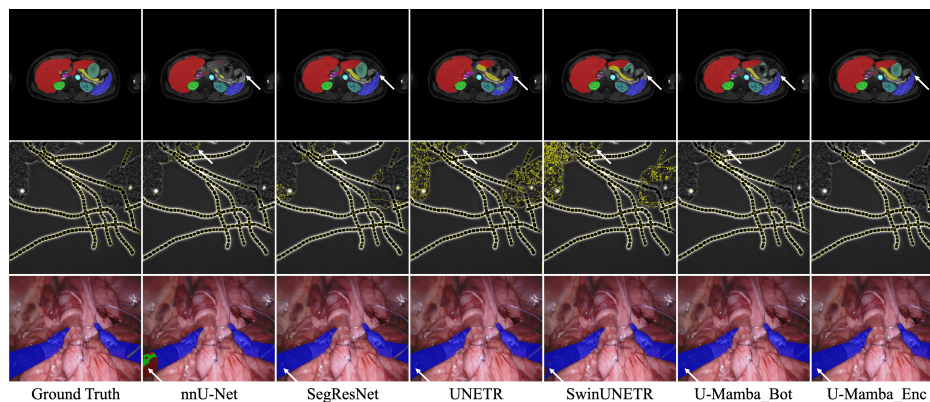
| Ground Truth | nnU-Net | SegResNet | UNETR | SwinUNETR | U-Mamba_Bot | U-Mamba_Enc |

Fig. 3. Visualized segmentation examples of abdominal organ segmentation MRI scans (1st row), cell segmentation in microscopy images (2nd row), and instruments segmentation in endoscopy images (3rd row). U-Mamba is more robust to heterogeneous appearances and has fewer segmentation outliers.

4   Discussion and conclusion

In this paper, we introduce U-Mamba to address the challenges in modeling long-range dependencies due to the inherent locality of CNNs and the computational complexity of Transformers. Comprehensive experimental results reveal that U-Mamaba outperforms existing CNN- and Transformer-based segmentation networks across diverse modalities and segmentation targets. In particular, U-Mamba has demonstrated superior capabilities in handling objects with heterogeneous appearances, resulting in fewer segmentation outliers. The performance gain is largely attributed to U-Mamba's architecture design, which can simultaneously extract multi-scale local features and capture long-range dependencies.

Transformers have demonstrated stronger performance on many natural image segmentation tasks [28]. However, they have not transformed medical image segmentation. This is evident as winning solutions in medical image segmentation competitions still predominantly rely on CNNs[6], such as nnU-Net [22] and SegResNet [39]. Interestingly, we also observed that Transformer-based networks underperform relative to CNN-based networks in all our tested scenarios, despite utilizing their original network implementations and training them with the recommended optimizers. This could be the requirement of training these networks with multiple GPUs rather than one GPU. However, this would lead to unfair comparisons because all the other networks were trained with only one GPU. Another reason could be that Transformers should be used in a large-scale pre-training and fine-tuning paradigm. To maintain consistency and fairness in our evaluation, we trained all networks from scratch and employed identical pre-

---

[6] https://github.com/JunMa11/SOTA-MedSeg

processing and data augmentation techniques across all experiments. We believe in the value of community collaboration and transparency, and therefore, we have made our implementations of the compared methods publicly available for further examination and use by the research community.

In addition, nnU-Net shows very competitive results on most tasks, but U-Mamba achieves overall better scores. We noticed that nnU-Net and U-Mamba have complementary segmentation performance for certain organs in CT and MRI scans, such as the aorta, kidneys, and inferior vena cava as shown in Appendix Table 5-7. This suggests the potential for further integrating them via the model ensemble, a strategy often employed to enhance performance in medical image segmentation competitions [30].

While the primary focus of this work is the new segmentation architecture, there are numerous avenues for further enhancement and expansion of U-Mamba. One immediate direction is to leverage large-scale datasets for train U-Mamba, aiming to create readily deployable segmentation tools or provide pre-trained model weights for fine-tuning on data-limited tasks, as exemplified by similar initiatives like TotalSegmentator [47] and STU-Net [21]. Furthermore, U-Mamba's design inherently supports integration with advanced techniques, such as strong data augmentations for small datasets, loss functions for highly imbalanced targets, and region-based training for nested objects [23]. In addition, U-Mamba block presents a new opportunity for application in classification and detection networks for better long-range dependency modeling. We leave these directions as near future work.

In conclusion, this paper presents a new architecture, U-Mamba, for general-purpose biomedical image segmentation, which integrates the advantages of local pattern recognition from CNNs and global context understanding from Mamba. U-Mamba can configure itself in an automatic way for different datasets, making it a versatile and flexible tool for diverse segmentation tasks in biomedical imaging. The results suggest that U-Mamba is a promising candidate to serve as the backbone of next-generation biomedical image segmentation networks.

References

1. Allan, M., Shvets, A., Kurmann, T., Zhang, Z., Duggal, R., Su, Y.H., Rieke, N., Laina, I., Kalavakonda, N., Bodenstedt, S., Herrera, L., Li, W., Iglovikov, V., Luo, H., Yang, J., Stoyanov, D., Maier-Hein, L., Speidel, S., Azizian, M.: 2017 robotic instrument segmentation challenge. arXiv preprint arXiv:1902.06426 (2019) 6, 11
2. Ba, J.L., Kiros, J.R., Hinton, G.E.: Layer normalization. arXiv preprint arXiv:1607.06450 (2016) 5

3. Bilic, P., Christ, P., Li, H.B., Vorontsov, E., Ben-Cohen, A., Kaissis, G., Szeskin, A., Jacobs, C., Mamani, G.E.H., Chartrand, G., Lohöfer, F., Holch, J.W., Sommer, W., Hofmann, F., Hostettler, A., Lev-Cohain, N., Drozdzal, M., Amitai, M.M., Vivanti, R., Sosna, J., Ezhov, I., Sekuboyina, A., Navarro, F., Kofler, F., Paetzold, J.C., Shit, S., Hu, X., Lipková, J., Rempfler, M., Piraud, M., Kirschke, J., Wiestler, B., Zhang, Z., Hülsemeyer, C., Beetz, M., Ettlinger, F., Antonelli, M., Bae, W., Bellver, M., Bi, L., Chen, H., Chlebus, G., Dam, E.B., Dou, Q., Fu, C.W., Georgescu, B., i Nieto, X.G., Gruen, F., Han, X., Heng, P.A., Hesser, J., Moltz, J.H., Igel, C., Isensee, F., Jäger, P., Jia, F., Kaluva, K.C., Khened, M., Kim, I., Kim, J.H., Kim, S., Kohl, S., Konopczynski, T., Kori, A., Krishnamurthi, G., Li, F., Li, H., Li, J., Li, X., Lowengrub, J., Ma, J., Maier-Hein, K., Maninis, K.K., Meine, H., Merhof, D., Pai, A., Perslev, M., Petersen, J., Pont-Tuset, J., Qi, J., Qi, X., Rippel, O., Roth, K., Sarasua, I., Schenk, A., Shen, Z., Torres, J., Wachinger, C., Wang, C., Weninger, L., Wu, J., Xu, D., Yang, X., Yu, S.C.H., Yuan, Y., Yue, M., Zhang, L., Cardoso, J., Bakas, S., Braren, R., Heinemann, V., Pal, C., Tang, A., Kadoury, S., Soler, L., van Ginneken, B., Greenspan, H., Joskowicz, L., Menze, B.: The liver tumor segmentation benchmark (lits). Medical Image Analysis **84**, 102680 (2023) 2

4. Campello, V.M., Gkontra, P., Izquierdo, C., Martín-Isla, C., Sojoudi, A., Full, P.M., Maier-Hein, K., Zhang, Y., He, Z., Ma, J., Parreño, M., Albiol, A., Kong, F., Shadden, S.C., Acero, J.C., Sundaresan, V., Saber, M., Elattar, M., Li, H., Menze, B., Khader, F., Haarburger, C., Scannell, C.M., Veta, M., Carscadden, A., Punithakumar, K., Liu, X., Tsaftaris, S.A., Huang, X., Yang, X., Li, L., Zhuang, X., Viladés, D., Descalzo, M.L., Guala, A., Mura, L.L., Friedrich, M.G., Garg, R., Lebel, J., Henriques, F., Karakas, M., Çavuş, E., Petersen, S.E., Escalera, S., Seguí, S., Rodríguez-Palomares, J.F., Lekadir, K.: Multi-centre, multi-vendor and multi-disease cardiac segmentation: The m&ms challenge. IEEE Transactions on Medical Imaging **40**(12), 3543–3554 (2021) 9

5. Chen, J., Lu, Y., Yu, Q., Luo, X., Adeli, E., Wang, Y., Lu, L., Yuille, A.L., Zhou, Y.: Transunet: Transformers make strong encoders for medical image segmentation. arXiv preprint arXiv:2102.04306 (2021) 2

6. Chen, J., Mei, J., Li, X., Lu, Y., Yu, Q., Wei, Q., Luo, X., Xie, Y., Adeli, E., Wang, Y., et al.: 3d transunet: Advancing medical image segmentation through vision transformers. arXiv preprint arXiv:2310.07781 (2023) 2

7. Chen, L.C., Zhu, Y., Papandreou, G., Schroff, F., Adam, H.: Encoder-decoder with atrous separable convolution for semantic image segmentation. In: Proceedings of the European Conference on Computer Vision. pp. 801–818 (2018) 2

8. Clark, K., Vendt, B., Smith, K., Freymann, J., Kirby, J., Koppel, P., Moore, S., Phillips, S., Maffitt, D., Pringle, M., Tarbox, L., Prior, F.: The cancer imaging archive (tcia): maintaining and operating a public information repository. Journal of Digital Imaging **26**(6), 1045–1057 (2013) 6, 11

9. Dosovitskiy, A., Beyer, L., Kolesnikov, A., Weissenborn, D., Zhai, X., Unterthiner, T., Dehghani, M., Minderer, M., Heigold, G., Gelly, S., et al.: An image is worth 16x16 words: Transformers for image recognition at scale. In: International Conference on Learning Representations (2020) 2, 4

10. Goel, K., Gu, A., Donahue, C., Ré, C.: It's raw! audio generation with state-space models. In: International Conference on Machine Learning. pp. 7616–7633 (2022) 2

11. Gu, A.: Modeling Sequences with Structured State Spaces. Phd thesis, Stanford University (2023), proQuest Document ID: 2880853867 2, 4

12. Gu, A., Dao, T.: Mamba: Linear-time sequence modeling with selective state spaces. arXiv preprint arXiv:2312.00752 (2023) 2, 4, 5, 11

13. Gu, A., Dao, T., Ermon, S., Rudra, A., Ré, C.: Hippo: Recurrent memory with optimal polynomial projections. In: Advances in Neural Information Processing Systems. vol. 33, pp. 1474–1487 (2020) 4

14. Gu, A., Goel, K., Re, C.: Efficiently modeling long sequences with structured state spaces. In: International Conference on Learning Representations (2021) 2, 4

15. Gu, A., Johnson, I., Goel, K., Saab, K., Dao, T., Rudra, A., Ré, C.: Combining recurrent, convolutional, and continuous-time models with linear state space layers. Advances in Neural Information Processing Systems **34**, 572–585 (2021) 2

16. Hatamizadeh, A., Nath, V., Tang, Y., Yang, D., Roth, H.R., Xu, D.: Swin UNETR: swin transformers for semantic segmentation of brain tumors in MRI images. In: International MICCAI Brainlesion Workshop. Lecture Notes in Computer Science, vol. 12962, pp. 272–284 (2021) 2, 7

17. Hatamizadeh, A., Tang, Y., Nath, V., Yang, D., Myronenko, A., Landman, B.A., Roth, H.R., Xu, D.: UNETR: transformers for 3d medical image segmentation. In: IEEE/CVF Winter Conference on Applications of Computer Vision. pp. 1748–1758 (2022) 2, 7

18. He, K., Zhang, X., Ren, S., Sun, J.: Deep residual learning for image recognition. In: Proceedings of the IEEE Conference on Computer Vision and Pattern Recognition. pp. 770–778 (2016) 5

19. Heller, N., Isensee, F., Maier-Hein, K.H., Hou, X., Xie, C., Li, F., Nan, Y., Mu, G., Lin, Z., Han, M., Yao, G., Gao, Y., Zhang, Y., Wang, Y., Hou, F., Yang, J., Xiong, G., Tian, J., Zhong, C., Ma, J., Rickman, J., Dean, J., Stai, B., Tejpaul, R., Oestreich, M., Blake, P., Kaluzniak, H., Raza, S., Rosenberg, J., Moore, K., Walczak, E., Rengel, Z., Edgerton, Z., Vasdev, R., Peterson, M., McSweeney, S., Peterson, S., Kalapara, A., Sathianathen, N., Papanikolopoulos, N., Weight, C.: The state of the art in kidney and kidney tumor segmentation in contrast-enhanced ct imaging: Results of the kits19 challenge. Medical Image Analysis **67**, 101821 (2021) 2

20. Hendrycks, D., Gimpel, K.: Gaussian error linear units (gelus). arXiv preprint arXiv:1606.08415 (2016) 5

21. Huang, Z., Wang, H., Deng, Z., Ye, J., Su, Y., Sun, H., He, J., Gu, Y., Gu, L., Zhang, S., Qiao, Y.: Stu-net: Scalable and transferable medical image segmentation models empowered by large-scale supervised pre-training. arXiv preprint arXiv:2304.06716 (2023) 11

22. Isensee, F., Jaeger, P.F., Kohl, S.A., Petersen, J., Maier-Hein, K.H.: nnu-net: a self-configuring method for deep learning-based biomedical image segmentation. Nature Methods **18**(2), 203–211 (2021) 2, 5, 7, 8, 10, 11

23. Isensee, F., Jäger, P.F., Full, P.M., Vollmuth, P., Maier-Hein, K.H.: nnu-net for brain tumor segmentation. In: International MICCAI Brainlesion Workshop. pp. 118–132 (2021) 11

24. Islam, M.M., Bertasius, G.: Long movie clip classification with state-space video models. In: European Conference on Computer Vision. pp. 87–104 (2022) 2

25. Ji, Y., Bai, H., GE, C., Yang, J., Zhu, Y., Zhang, R., Li, Z., Zhanng, L., Ma, W., Wan, X., Luo, P.: AMOS: A large-scale abdominal multi-organ benchmark for versatile medical image segmentation. In: Neural Information Processing Systems: Datasets and Benchmarks Track (2022) 6, 11

26. Kingma, D.P., Ba, J.: Adam: A method for stochastic optimization. In: International Conference on Learning Representations (2015) 8

27. LeCun, Y., Bengio, Y.: Convolutional Networks for Images, Speech, and Time Series, p. 255–258. MIT Press, Cambridge, MA, USA (1998) 2

28. Liu, Z., Lin, Y., Cao, Y., Hu, H., Wei, Y., Zhang, Z., Lin, S., Guo, B.: Swin transformer: Hierarchical vision transformer using shifted windows. In: Proceedings of the IEEE/CVF International Conference on Computer Vision. pp. 10012–10022 (2021) 2, 4, 10

29. Loshchilov, I., Hutter, F.: Decoupled weight decay regularization. In: International Conference on Learning Representations (2019) 8

30. Ma, J.: Cutting-edge 3d medical image segmentation methods in 2020: Are happy families all alike? arXiv preprint arXiv:2101.00232 (2021) 11

31. Ma, J., Chen, J., Ng, M., Huang, R., Li, Y., Li, C., Yang, X., Martel, A.L.: Loss odyssey in medical image segmentation. Medical Image Analysis **71**, 102035 (2021) 7

32. Ma, J., He, Y., Li, F., Han, L., You, C., Wang, B.: Segment anything in medical images. arXiv preprint arXiv:2304.12306 (2023) 6

33. Ma, J., Wang, B.: Towards foundation models of biological image segmentation. Nature Methods **20**(7), 953–955 (2023) 1

34. Ma, J., Xie, R., Ayyadhury, S., Ge, C., Gupta, A., Gupta, R., Gu, S., Zhang, Y., Lee, G., Kim, J., Lou, W., Li, H., Upschulte, E., Dickscheid, T., de Almeida, J.G., Wang, Y., Han, L., Yang, X., Labagnara, M., Rahi, S.J., Kempster, C., Pollitt, A., Espinosa, L., Mignot, T., Middeke, J.M., Eckardt, J.N., Li, W., Li, Z., Cai, X., Bai, B., Greenwald, N.F., Valen, D.V., Weisbart, E., Cimini, B.A., Li, Z., Zuo, C., Brück, O., Bader, G.D., Wang, B.: The multi-modality cell segmentation challenge: Towards universal solutions. arXiv:2308.05864 (2023) 2, 6, 7, 11

35. Ma, J., Zhang, Y., Gu, S., Ge, C., Ma, S., Young, A., Zhu, C., Meng, K., Yang, X., Huang, Z., Zhang, F., Liu, W., Pan, Y., Huang, S., Wang, J., Sun, M., Xu, W., Jia, D., Choi, J.W., Alves, N., de Wilde, B., Koehler, G., Wu, Y., Wiesenfarth, M., Zhu, Q., Dong, G., He, J., the FLARE Challenge Consortium, Wang, B.: Unleashing the strengths of unlabeled data in pan-cancer abdominal organ quantification: the flare22 challenge. arXiv preprint arXiv:2308.05862 (2023) 2, 6, 11

36. Maas, A.L., Hannun, A.Y., Ng, A.Y., et al.: Rectifier nonlinearities improve neural network acoustic models. In: International Conference on Machine Learning. vol. 28 (2013) 5

37. Maier-Hein, L., Reinke, A., Godau, P., Tizabi, M.D., Büttner, F., et al.: Metrics reloaded: Pitfalls and recommendations for image analysis validation. arXiv preprint arXiv:2206.01653 (2022) 8

38. Minaee, S., Boykov, Y., Porikli, F., Plaza, A., Kehtarnavaz, N., Terzopoulos, D.: Image segmentation using deep learning: A survey. IEEE Transactions on Pattern Analysis and Machine Intelligence **44**(7), 3523–3542 (2021) 1

39. Myronenko, A.: 3d MRI brain tumor segmentation using autoencoder regularization. In: International MICCAI Brainlesion Workshop. Lecture Notes in Computer Science, vol. 11384, pp. 311–320 (2018) 7, 10

40. Nguyen, E., Goel, K., Gu, A., Downs, G., Shah, P., Dao, T., Baccus, S., Ré, C.: S4nd: Modeling images and videos as multidimensional signals with state spaces. In: Advances in Neural Information Processing Systems. vol. 35, pp. 2846–2861 (2022) 2

41. Ronneberger, O., Fischer, P., Brox, T.: U-net: Convolutional networks for biomedical image segmentation. In: International Conference on Medical image computing and computer-assisted intervention. pp. 234–241 (2015) 2, 5

42. Simpson, A.L., Antonelli, M., Bakas, S., Bilello, M., Farahani, K., van Ginneken, B., Kopp-Schneider, A., Landman, B.A., Litjens, G., Menze, B., Ronneberger, O., Summers, R.M., Bilic, P., Christ, P.F., Do, R.K.G., Gollub, M., Golia-Pernicka, J., Heckers, S.H., Jarnagin, W.R., McHugo, M.K., Napel, S., Vorontsov, E., Maier-Hein, L., Cardoso, M.J.: A large annotated medical image dataset for the development and evaluation of segmentation algorithms. arXiv preprint arXiv:1902.09063 (2019) 6, 11

43. Stringer, C., Wang, T., Michaelos, M., Pachitariu, M.: Cellpose: a generalist algorithm for cellular segmentation. Nature Methods **18**(1), 100–106 (2021) 2

44. Tay, Y., Dehghani, M., Abnar, S., Shen, Y., Bahri, D., Pham, P., Rao, J., Yang, L., Ruder, S., Metzler, D.: Long range arena: A benchmark for efficient transformers. In: International Conference on Learning Representations (2020) 4

45. Ulyanov, D., Vedaldi, A., Lempitsky, V.: Instance normalization: The missing ingredient for fast stylization. arXiv preprint arXiv:1607.08022 (2016) 5

46. Vaswani, A., Shazeer, N., Parmar, N., Uszkoreit, J., Jones, L., Gomez, A.N., Kaiser, Ł., Polosukhin, I.: Attention is all you need. Advances in neural Information Processing Systems **30** (2017) 2, 4

47. Wasserthal, J., Breit, H.C., Meyer, M.T., Pradella, M., Hinck, D., Sauter, A.W., Heye, T., Boll, D.T., Cyriac, J., Yang, S., Bach, M., Segeroth, M.: Totalsegmentator: Robust segmentation of 104 anatomic structures in ct images. Radiology: Artificial Intelligence **5**(5) (2023) 11

48. Yushkevich, P.A., Gao, Y., Gerig, G.: Itk-snap: An interactive tool for semi-automatic segmentation of multi-modality biomedical images. In: Annual International Conference of the IEEE Engineering in Medicine and Biology Society. pp. 3342–3345 (2016) 6

49. Zhou, H.Y., Guo, J., Zhang, Y., Han, X., Yu, L., Wang, L., Yu, Y.: nnformer: volumetric medical image segmentation via a 3d transformer. IEEE Transactions on Image Processing **32**, 4036–4045 (2023) 2

Appendix

Table 5. Organ-wise segmentation results of 3D models in abdomen CT dataset. The best and the second-best scores for each organ and each metric are highlighted in red and blue, respectively. (IVC: Inferior vena cava, RAG: Right adrenal gland, LAG: Left adrenal gland)

Organs	nnU-Net		SegResNet		UNETR		SwinUNETR		U-Mamba Bot		U-Mamba Enc	
	DSC	NSD	DSC	NSD	DSC	NSD	DSC	NSD	DSC	NSD	DSC	NSD
Liver	0.9706	0.9582	0.9521	0.9157	0.9047	0.8125	0.9302	0.8297	0.9713	0.9592	0.9714	0.9578
Right kidney	0.8738	0.8621	0.8295	0.8027	0.7105	0.6609	0.7540	0.7053	0.8653	0.8640	0.8864	0.8733
Spleen	0.9162	0.9038	0.8646	0.8421	0.7869	0.7347	0.8402	0.802	0.9357	0.9361	0.9241	0.9241
Pancreas	0.8362	0.9139	0.7440	0.8353	0.6010	0.6859	0.6973	0.7191	0.8651	0.9402	0.8407	0.9157
Aorta	0.9618	0.9745	0.9491	0.9558	0.8916	0.8701	0.9383	0.9340	0.9570	0.9727	0.9445	0.9567
IVC	0.8839	0.8776	0.8374	0.8242	0.7592	0.7199	0.8250	0.7834	0.8822	0.8784	0.8748	0.8697
RAG	0.8231	0.9318	0.7277	0.8579	0.6373	0.7615	0.7466	0.8703	0.8140	0.9236	0.7827	0.8886
LAG	0.7921	0.8884	0.6851	0.7945	0.4750	0.5866	0.6767	0.7888	0.8323	0.9258	0.8206	0.9159
Gallbladder	0.7293	0.7331	0.6678	0.6411	0.5321	0.4747	0.5725	0.5320	0.7436	0.7467	0.7767	0.7786
Esophagus	0.8606	0.9308	0.7927	0.8706	0.6929	0.7826	0.7853	0.8663	0.8523	0.9149	0.8689	0.9323
Stomach	0.8902	0.9033	0.8207	0.8302	0.7128	0.6903	0.7656	0.6981	0.8931	0.9076	0.8856	0.9034
Duodenum	0.7561	0.8830	0.6388	0.7961	0.4951	0.6932	0.6042	0.7531	0.7794	0.8930	0.7534	0.8692
Left kidney	0.9050	0.9035	0.7949	0.7686	0.6724	0.6324	0.7367	0.6799	0.8963	0.9019	0.8991	0.8889
Average	0.8615	0.8972	0.7926	0.8258	0.6824	0.7004	0.7594	0.7663	0.8683	0.9049	0.8638	0.8980

Table 6. Organ-wise segmentation results of 3D models in abdomen MRI dataset. The best and the second-best scores for each organ and each metric are highlighted in red and blue, respectively. (IVC: Inferior vena cava, RAG: Right adrenal gland, LAG: Left adrenal gland)

Organs	nnU-Net		SegResNet		UNETR		SwinUNETR		U-Mamba Bot		U-Mamba Enc	
	DSC	NSD	DSC	NSD	DSC	NSD	DSC	NSD	DSC	NSD	DSC	NSD
Liver	0.9735	0.9747	0.9654	0.9590	0.9344	0.8905	0.9627	0.9479	0.9732	0.9753	0.9717	0.9704
Right kidney	0.9625	0.9747	0.9390	0.9588	0.8266	0.8228	0.9355	0.9390	0.9594	0.9766	0.9621	0.9800
Spleen	0.9131	0.9201	0.9023	0.9069	0.8617	0.8280	0.9134	0.9019	0.9383	0.9417	0.9442	0.9468
Pancreas	0.8639	0.9553	0.8249	0.9228	0.7271	0.8268	0.7750	0.8742	0.8650	0.9565	0.8623	0.9560
Aorta	0.9327	0.9572	0.9331	0.9556	0.8524	0.8652	0.8907	0.9055	0.9243	0.9479	0.9467	0.9711
IVC	0.8192	0.8698	0.8279	0.8762	0.7286	0.7605	0.7844	0.8271	0.8322	0.8812	0.8230	0.8740
RAG	0.6238	0.8047	0.6066	0.7778	0.4539	0.6257	0.5540	0.7316	0.6287	0.8010	0.6438	0.8197
LAG	0.7021	0.8474	0.6779	0.8301	0.4735	0.6143	0.4786	0.6255	0.7225	0.8588	0.7419	0.8713
Gallbladder	0.7720	0.7551	0.7872	0.7581	0.4833	0.4095	0.6537	0.6185	0.8284	0.8279	0.8503	0.8449
Esophagus	0.7489	0.9071	0.7408	0.8976	0.5655	0.7395	0.6477	0.8038	0.7955	0.9387	0.7890	0.9369
Stomach	0.8260	0.8595	0.7609	0.7989	0.6697	0.6919	0.7198	0.7553	0.8257	0.8597	0.8283	0.8679
Duodenum	0.7008	0.8892	0.6634	0.8720	0.4878	0.7495	0.5921	0.8148	0.7309	0.9078	0.7232	0.8991
Left kidney	0.9637	0.9805	0.9609	0.9798	0.8622	0.8479	0.9266	0.9377	0.9649	0.9842	0.9647	0.9842
Average	0.8309	0.8996	0.8146	0.8841	0.6867	0.7440	0.7565	0.8218	0.8453	0.9121	0.8501	0.9171

Table 7. Organ-wise segmentation results of 2D models in abdomen MRI dataset. The best and the second-best scores for each organ and each metric are highlighted in red and blue, respectively. (IVC: Inferior vena cava, RAG: Right adrenal gland, LAG: Left adrenal gland)

Organs	nnU-Net		SegResNet		UNETR		SwinUNETR		U-Mamba Bot		U-Mamba Enc	
	DSC	NSD	DSC	NSD	DSC	NSD	DSC	NSD	DSC	NSD	DSC	NSD
Liver	0.9478	0.9286	0.9321	0.9051	0.8988	0.8173	0.9484	0.9108	0.9534	0.9319	0.9579	0.9390
Right kidney	0.8782	0.8749	0.8957	0.8802	0.6974	0.6606	0.8598	0.8391	0.9039	0.8922	0.9070	0.9043
Spleen	0.9043	0.8956	0.8793	0.8573	0.7182	0.6612	0.8922	0.8649	0.9065	0.8992	0.9137	0.9065
Pancreas	0.7148	0.8398	0.6998	0.8257	0.5679	0.6990	0.7049	0.8260	0.7376	0.8577	0.7500	0.8715
Aorta	0.9214	0.9465	0.9333	0.9582	0.8294	0.8401	0.8750	0.8929	0.9257	0.9571	0.9122	0.9409
IVC	0.7567	0.8045	0.7527	0.8003	0.6310	0.6703	0.7105	0.7536	0.7653	0.8136	0.7631	0.8147
RAG	0.4960	0.6743	0.4746	0.6755	0.3478	0.5243	0.4552	0.6162	0.5513	0.7338	0.5371	0.7293
LAG	0.5419	0.7023	0.5542	0.7089	0.3471	0.4764	0.4758	0.6221	0.5682	0.7283	0.5642	0.7163
Gallbladder	0.6807	0.6371	0.6256	0.5959	0.3103	0.2557	0.6034	0.5581	0.6664	0.6355	0.6762	0.6413
Esophagus	0.6964	0.8605	0.6756	0.8542	0.5648	0.7602	0.6347	0.8216	0.7042	0.8633	0.7025	0.8669
Stomach	0.7351	0.7622	0.7134	0.7437	0.5583	0.5756	0.6739	0.6945	0.7420	0.7636	0.7680	0.7888
Duodenum	0.5204	0.7842	0.4784	0.7450	0.3054	0.6156	0.4448	0.7335	0.5295	0.7890	0.5516	0.7952
Left kidney	0.8911	0.8881	0.898	0.8943	0.6944	0.6459	0.8580	0.8361	0.9100	0.9058	0.9084	0.9106
Average	0.7450	0.8153	0.7317	0.8034	0.5747	0.6309	0.7028	0.7669	0.7588	0.8285	0.7625	0.8327